ELSEVIER

Remote Sensing of Environment 79 (2002) 225–242

Remote Sensing of Environment

www.elsevier.com/locate/rse

Evaluating land surface moisture conditions from the remotely sensed temperature/vegetation index measurements An exploration with the simplified simple biosphere model

Samuel N. Goward[a,*], Yongkang Xue[b], Kevin P. Czajkowski[c]

[a]*Laboratory for Global Remote Sensing Studies, Department of Geography, University of Maryland, College Park, MD 20742, USA*
[b]*Department of Geography, University of California at Los Angles, Los Angles, CA 91320, USA*
[c]*Department of Geography and Planning, University of Toledo, Toledo, OH 43606, USA*

Received 2 December 1999; received in revised form 6 November 2000; accepted 28 November 2000

Abstract

Land soil moisture conditions play a critical role in evaluating terrestrial environmental conditions related to ecological, hydrological, and atmospheric processes. Extensive efforts to exploit the potential of remotely sensed observations to help quantify this complex variable are still underway. Among the various methods, several investigators have explored a combination of surface temperatures and spectral vegetation index (SVI) measurements, the TVX method, as a means to account for the variable influence of vegetation cover in soil moisture assessment. Although considerable empirical evidence has been presented exploring the potential of TVX methods to assess regional moisture conditions, less attention has been given to assessing the underlying biophysics of the observed TVX patterns. In this study, the Simplified Simple Biosphere (SSiB) model is exploited to examine the factors that lead to the observed TVX relation. For a range of typical, midlatitude, growing season conditions, the SSiB model produces the expected TVX relationship, surface temperature decreases with increasing SVI values. The most critical factors that cause the TVX relation to vary include near-surface soil moisture (2 cm), incident radiation (IR), and, to a lesser degree, wind speed. Whereas many empirical studies have suggested that the slope of the TVX relation may provide an important diagnostic of soil moisture conditions, in this analysis, the impact of plant stomatal function is shown to confuse this interpretation of the TVX slope. However, other aspects of the TVX metrics, specifically bare soil temperature and canopy temperature, do provide diagnostic near-surface soil moisture information. Growing season variations in TVX metrics were examined for the conditions recorded at the Hydrological and Atmospheric Pilot Experiment — Modelisation du Bilan Hydrique (HAPEX-Mobilhy) study site. The results from this analysis indicate that soil and canopy temperatures vary as a function of soil moisture conditions and, to a lesser degree, as a result of varying solar insolation and wind speed. The results also show that the TVX metrics are able to provide daily soil moisture variation up to 2 cm of soil depth and seasonal trend up to 10 cm. Using the satellite-derived surface temperatures and a SSiB-derived retrieval equation, the retrieved soil moistures at the HAPEX-Mobilhy site generally closely approximate the conditions recorded on the ground.

1. Introduction

One of the most important land environmental variables, relative to land surface climatology, hydrology, and ecology, is soil moisture (Sellers & Schimel, 1993). Variations in soil moisture produce significant changes in surface energy balance, regional runoff, and vegetation productivity. Accurate assessment of this variable is difficult both because typical field methods are complex and expensive and local scale variations in soil properties, terrain, and vegetation cover make selection of representative field sites difficult if not impossible (Engman & Chauhan, 1997; Wood, 1997).

Remotely sensed observations of reflected and emitted electromagnetic (EM) radiation appear to be at least a partial solution to the spatial sampling problem. Imaging sensors, flown on aircraft and spacecraft, provide the capability to produce spatially comprehensive measurements of surface environmental conditions. If variations in measured EM existence can be related to surface moisture conditions, then both regional variations and local spatial heterogeneity of soil moisture conditions may be recorded (Chen, Engman,

* Corresponding author. Tel.: +1-301-405-4050; fax: +1-301-314-9299.
E-mail address: sg21@umail.umd.edu (S.N. Goward).

0034-4257/01/$ – see front matter © 2002 Elsevier Science Inc. All rights reserved.
PII: S0034-4257(01)00275-9

& Brutsaert, 1997; Dubayah, Wood, & Lavallee, 1996; Kustas, Perry, Doriswamy, & Moran, 1994).

Over the last quarter century, substantial research has been dedicated to the use of remotely sensed observations to evaluate soil moisture conditions. Studies, which employ measurements from solar reflectance (Curran, 1981; Hardy, 1980), thermal infrared wavelengths (Carlson, Dodd, Benjamin, & Cooper, 1981; Goward, Waring, Dye, & Yang, 1994; Heilman, Kanemasu, Rosenberg, & Blad, 1976; Norman, Divakarla, & Goel, 1995; Price, 1980), and microwave (Kasischke, Melack, & C., 1997; Njoku & Entekhabi, 1996), have all shown some potential in this area. Problems encountered in estimating surface wetness conditions originate from the diversity of EM sources recorded in a single measurement (e.g., soil, vegetation leaves and woody material, litter, etc.), the range of forcing variables that can determine the current EM exitance (e.g., surface moisture, incident radiation (IR), wind, albedo, thermal inertia, etc.), and the transfer of emitted radiation through the atmosphere. In general, derivation of a relation between surface moisture and EM exitance is an underdetermined problem, with unknowns substantially exceeding the acquired measurements.

Recent progress in applications of remote sensing to soil moisture assessment suggest that a combination of measurement approaches may provide more robust results (Anderson, Norman, Diak, Kustas, & Mecikalski, 1997; Chanzy, Bruckler, & Perrier, 1995; Hope & McDowell, 1992; Moran et al., 1997; Theis, Blancher, & Newton, 1984). This study explores the biophysics of one such "combined" method, the temperature/vegetation index (TVX) approach, which analyzes a spatial or contextual array of remotely sensed spectral solar reflective and thermal infrared measurements to estimate near-surface soil moisture conditions (Goward, Cruickshanks, & Hope, 1985; Price, 1990).

2. Background

One approach to solving the underdetermination of soil moisture from remotely sensed observations is to employ spatial or contextual arrays as a means to increase the measurement domain (Chen et al., 1997; Price, 1990; Prihodko & Goward, 1997). Empirical evidence has repeatedly demonstrated that surface radiometric temperatures, measured in the 8- to 14-μm spectral region, are correlated with visible/near-infrared SVIs as well as visible wavelength measurements (Carlson, Gilles, & Perry, 1994; Carlson, Perry, & Schmugge, 1990; Czajkowski, Goward, Chilar, Dubayah, & Mulhern, 1997; Czajkowski, Goward, Stadler, & Waltz, 2000; Friedl & Davis, 1994; Goetz, 1997; Goward et al., 1985, 1994; Hope, Petzold, Goward, & Ragan, 1987; Nemani, Pierce, Running, & Goward, 1993; Nemani & Running, 1989; Price, 1990; Smith & Choudhury, 1991). To simplify discussion, we call this the TVX approach to land surface environmental analysis (Goetz, 1997; Prihodko & Goward, 1997) (Fig. 1).

Variations in the slope and intercepts of this empirical TVX correlation, from daytime optical and thermal infrared remotely sensed measurements, have variously been attributed to surface evapotranspiration (Hope et al., 1987), canopy conductance (Nemani & Running, 1989), moisture availability (Carlson et al., 1990), and surface soil moisture (Friedl & Davis, 1994). The physical bases for these possible explanations have been pursued in previous work, but no detailed factor analysis of what determines the pattern and variations in the TVX relation has been reported.

2.1. The remotely sensed phenomena

The surface temperature (T_s), spectral vegetation index (SVI) correlation, is indicative of how vegetation foliar cover modulates remotely sensed T_s measurements. SVIs, such as the normalized difference vegetation index (NDVI) or simple ratio (SR), have variously been shown to relate to percentage green vegetation cover, leaf area index (LAI), and green biomass (Curran, 1983; Jackson, 1983; Tucker, 1979). Land materials such as bare soil and vegetation foliage are opaque in the thermal infrared portion of the spectrum. Thus, a remotely sensed TIR measurements records the radiometric temperature of the land surface materials directly in the field of view of the sensor (e.g., there is no scatter or transmission of TIR radiation from underlying materials) (Hatfield, 1979; Hunt, 1973; Smith, Ranson, Nguyen, & Balick, 1985). As a SVI measurement increases, the amount of green foliage observed by the sensor increases and the radiometic temperature recorded more closely approximates the temperature of green leaves. At spectral vegetation maximum (e.g., an optically infinitely thick vegetation canopy) or complete canopy closure, the T_s measurement records the canopy temperature (T_c). At the

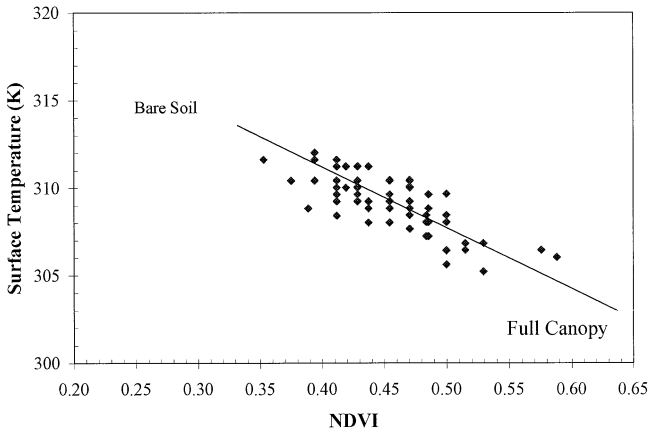

Fig. 1. Example TVX plot from AVHRR 2:30 p.m. observations for HAPEX-Mobilhy study area. Note the inverse relation between surface temperature and the NDVI. The contextual data structure is typically observed in these midafternoon observations.

other extreme of 0% vegetation cover, the T_s measurement typically records the radiometric temperature of sunlit nonvegetated surfaces, such as bare soil (T_g). Reduced to simplest terms, the end points of the TVX correlation are nonvegetated bare surfaces such as soil (T_g) and canopy temperature (T_c).

2.2. Biophysics of TVX variations

Daytime variations in T_g and T_c as well as differences between these two temperatures are a complex function of current and preceding meteorological conditions and current physical conditions of the land surface. In fact, explanation of the observed TVX variations is a fundamental problem in land boundary meteorology because it requires a thorough understanding of what causes T_g and T_c to vary and differ from one another. Biophysical land surface conditions, such as vegetation cover, stomatal functioning, albedo, soil moisture, and thermal inertia, interact with IR, air flow, and other atmospheric variables to produce energy and mass exchange at this boundary layer, which in turn determines soil and canopy temperatures as well as near-surface air temperatures. Meteorological observations in this near-surface boundary layer have shown that vegetation foliage temperature (T_c) equilibrates closely to air temperature (T_a), whereas T_s of nonvegetated (e.g., sunlit, bare soil) surfaces (T_g) is typically warmer than T_c and varies significantly with environmental conditions such as surface moisture and IR (Geiger, 1965). Our previous research substantiated that, within the limits of the Advanced Very High Resolution Radiometer (AVHRR) system to accurately estimate T_s (Cooper & Asrar, 1989), T_s measurement derived for closed canopy vegetation is a good approximation of T_a (Prihodko & Goward, 1997). In this study, we explore further the potential of other TVX metrics including the T_g estimate and the difference between T_g and T_c as an estimate of the slope of the TVX relation, as potential diagnostics of soil moisture conditions. However, as a boundary layer diagnostic, the TVX relation should be sensitive to all relevant conditions and processes, rather than a single variable such as soil moisture. Thus, in order to understand the value of the TVX method in soil moisture assessment, the role of other variables in determining this relation must also be considered.

3. Approach

In this study, we employ the Simplified Simple Biosphere (SSiB) model (Xue, Sellers, Kinter, & Shukla, 1991) to explore the physical bases of the TVX relation. The SSiB model performs numerical simulation of land/atmosphere interactions based on the principals of energy and water conservation. SSiB was originally developed as the land boundary layer component for climate simulations but with the appropriate atmospheric observations can be run independent of the related atmospheric model. From known or modeled atmospheric conditions, SSiB produces surface fluxes and surface environmental conditions such as soil moisture. SSiB was developed based on comparisons against observational data and a large number of field measurements have been used to validate and calibrate the model (Xue, Bastable, Dirmeyer, & Sellers, 1996; Xue et al., 1991; Xue, Zeng, & Schlosser, 1996).

For this study, we employed observations from the Hydrological and Atmospheric Pilot Experiment—Modelisation du Bilan Hydrique (HAPEX-Mobilhy) field study to drive the SSiB model. This site in east, central France has been subjected to detailed land surface climatological research and, as such, provides the wide range of variables and conditions needed to examine the TVX method. The vegetation canopy cover at this site is a soybean crop. The optical and structural aspects of soybeans are well understood in remote sensing research, and thus present an ideal subject for this exploratory analysis (Holben, Tucker, & Fan, 1980).

The first step in our analysis examines how sunlit soil temperatures (T_g) and canopy foliar temperatures (T_c), as well as differences between them, vary as a function of near-surface soil moisture, IR, wind speed, and atmospheric vapor pressure deficit. From the perspective of soil moisture estimation, ideally, the only important factor determining T_g and T_c, or differences between them, would be soil moisture. However, the other environmental factors could easily confuse or convolute any such potential. To carry out this analysis, we examine a typical midlatitude summer day, varying one environmental factor at time to assess TVX sensitivity to each environmental condition (Table 1).

Given this understanding, we then considered the potential of inferring soil moisture with remotely sensed TVX metrics by calculating the 2:00 p.m. TVX metrics for each day during the growing season (May to September) and comparing these metrics with soil moisture variations and other variables. To do so, we ran the model using half-hourly field measurements collected over the growing season during HAPEX-Mobilhy field study. We did not explore the conditions during the October to April time period because of the absence of the soybean vegetation canopy during this time period.

We also explored the use of the model-derived TVX relations to extract surface soil moisture estimates from selected AVHRR satellite remotely sensed observations acquired during the HAPEX-Mobilhy field study.

Table 1
Environmental conditions used in calculations

	Minimum	Maximum	Increment	Control experiment
VSW[1]	4%	45%	3%	15%
IR (W/m^2)	650	1400	50	1100
Wind speed (m/s)	0.4	5.0	0.5	1.7

[1] (Volumetric Soil Water Content).

3.1. The SSiB model

In a stand alone mode (i.e., not coupled to atmospheric models), a set of forcing data, including precipitation, downward short- and long-wave radiation, air temperature, humidity, and wind at reference height, are required to drive SSiB. About 20 vegetation and soil parameters are also needed to specify land surface condition. The major parameters include vegetation cover, LAI, and its green fraction, albedo, surface roughness length and zero displacement height, soil conductivity and soil water potential at saturation, wilting point, and some parameters of stomatal resistance that relate to environmental factors (e.g., water vapor deficit and soil moisture). Using the forcing data and specified vegetation and soil conditions, SSiB produces latent and sensible heat fluxes, momentum flux, carbon flux, runoff, and prognostic variables, including soil moisture, soil temperature, and canopy temperature.

Within SSiB, there are three soil layers, one canopy layer and eight prognostic variables, including the soil wetness for the three soil layers (0.02, 0.48, and 1.1 m), water content retained by the canopy, snow on the ground, and canopy temperature. There are two soil temperatures: soil surface temperature and deep soil temperature, which are obtained using the force-restore method. The model uses stomatal resistance (R_c), soil resistance (R_{soil}), and canopy boundary layer resistance (R_b), and two aerodynamic resistances to control the exchanges of momentum, heat, and water between the atmosphere and land surface (Fig. 2).

The governing equation for canopy temperature T_c is based on an energy conservation equation (Eq. (1)).

$$C_c \frac{\partial_c}{\partial t} = R_{nc} - H_c - \lambda E_c \tag{1}$$

where C_c, R_{nc}, H_c, and λE_c are heat capacity of canopy, net radiation, sensible heat flux, and latent heat flux at the canopy level, respectively. The force-restore method is used to predict the time variation of the ground temperature T_g (Eq. (2)).

$$C_{gs} \frac{\partial T_{gs}}{\partial t} = R_{ngs} - H_{gs} - \lambda E_{gs} - \frac{2\pi C_{gs}}{\tau}(T_{gs} - T_d) \tag{2}$$

where τ is the day length, C_{gs} the effective heat capacity of soil, T_d the temperature for deep soil, and R_{ngs}, H_{gs}, and λE_{gs} are net radiation, sensible heat flux, and latent heat flux at the ground, respectively. The changes in each component of these two equations would affect T_c and T_g. In the three soil layers, water movement is described by

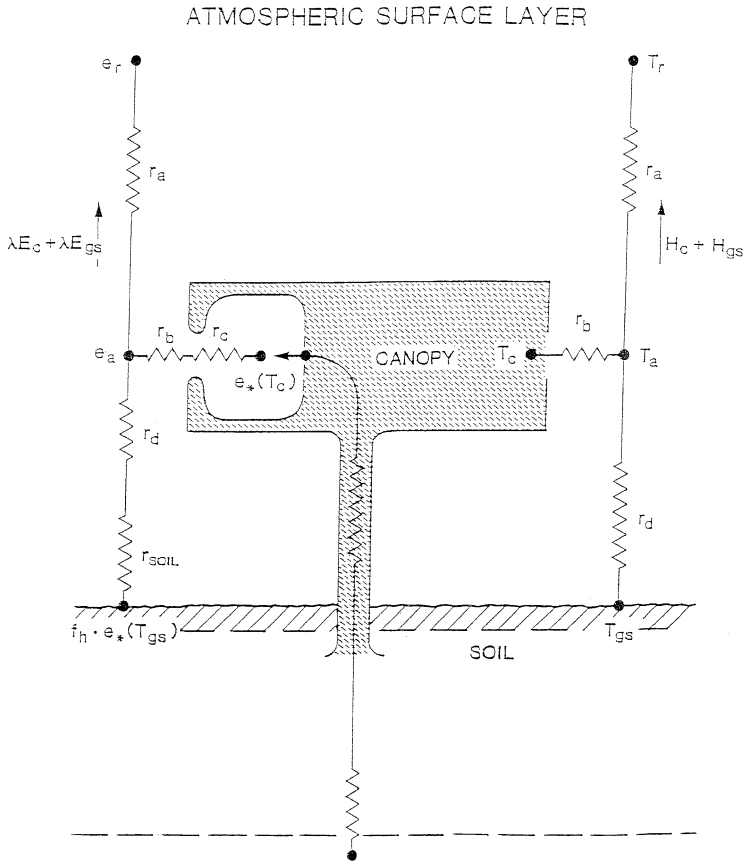

Fig. 2. Schematic diagram of the SSiB model structure. The symbols are defined in the text.

the finite-difference approximation to the diffusion equations. The soil moisture equation for the first soil layer is (Eq. (3)):

$$\frac{\partial \theta_1}{\partial t} = \frac{1}{D_1}[P + Q_{12} - E_{gs} - b_1 E_c] \quad (3)$$

where P is the precipitation reaching the ground, θ_1 and D_1 are the volumetric soil water content (VSW) and soil thickness of the top soil layers, respectively. The fraction factor b_1 depends on the root distribution of the top soil layer, Q_{12} is the transfer of water between the first and second layers, and E_c is the evaporation from the canopy. The above equations show that there are close relationships between T_c, T_g, and θ_1, which is the physical basis for the TVX relation and will be elaborated further later in the paper.

The stand-alone version of SSiB has been validated and calibrated using data measured from various vegetation types and regions in the world. In the stand-alone version, field measurements specify the atmospheric conditions that serve as the driving force in SSiB. Fluxes, surface temperature, soil moisture, and other variables simulated by SSiB are compared with observations. The data used for the validations include the Amazon rainforest data (Xue et al., 1991), the Russian soil moisture data (Robock, Vinnikov, Schlosser, Speranskaya, & Xue, 1995; Schlosser, Robock, Vinnikov, Speranskaya, & Xue, 1997), the HAPEX-Mobilhy data from a crop site in France (Xue, Zeng, et al., 1996), the Cabauw data from a grassland site in the Netherlands (Chen et al., 1996), the Anglo–Brazilian Amazonian Climate Observation (ABRACOS) data from a deforestation site in the Amazon (Xue, Bastable, et al., 1996), and the Sahelian Energy Balance Experiment (SEBEX) and the Hydrologic Pilot Experiment in the Sahel (HAPEX-Sahel) field measurement data from a semiarid site in Niger (Xue, Allen, & Li, 1996; Xue, Zeng, Schlosser, & Allen, 1998), the First ISLSCP International Satellite Land-Surface Climatology Project Field Experiment (FIFE) data, a grassland site in Kansas (Chen et al., 1996), and the Red-Arkansas River Basin data in the southern Great Plains of the US (Wood et al., 1998). Some of the abovementioned studies are part of the Project for Intercomparison of Land-Surface Parameterization Scheme (PILPS; Henderson-Sellers & Brown, 1992). Model validation has played a significant role in the development of a physically based land surface model.

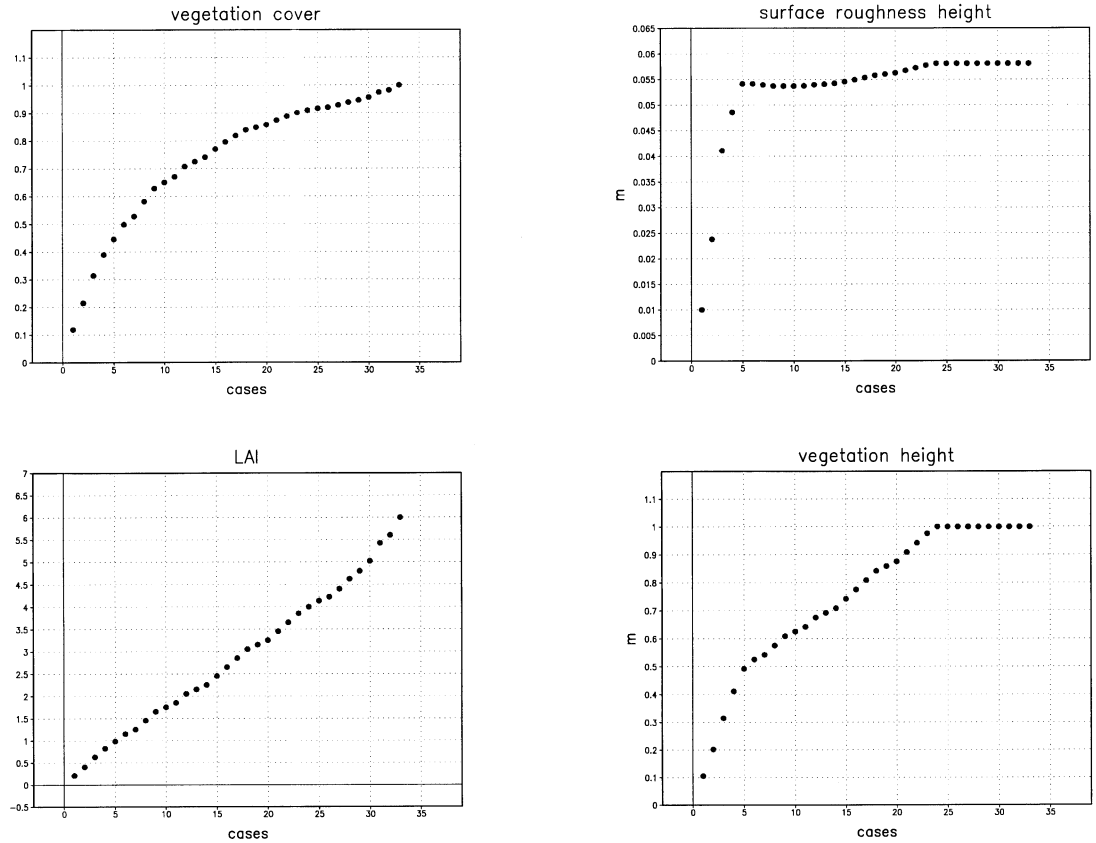

Fig. 3. The HAPEX-Mobilhy PILPS field measurements of (a) percentage vegetation cover, (b) LAI, (c) surface roughness height, and (d) vegetation height observed for the soy crop canopy from May to September.

3.2. The HAPEX-Mobilhy study site

HAPEX-Mobilhy was an multinational scientific experiment supported by the French Direction de la Meteorologié (DMN), Programme National d'Etude de la Dynamique du Climat (PNEDC), and the Institut National de la Recherche Agronomique (INRA). Participants from the United States include scientists from the National Center for Atmospheric Research (NCAR) and NASA.

Data were obtained from HAPEX-Mobilhy at Caumont (SAMER No. 3, 43°41′N, 0°6′W, mean elevation 113 m). Detailed information on the SAMER network and the site

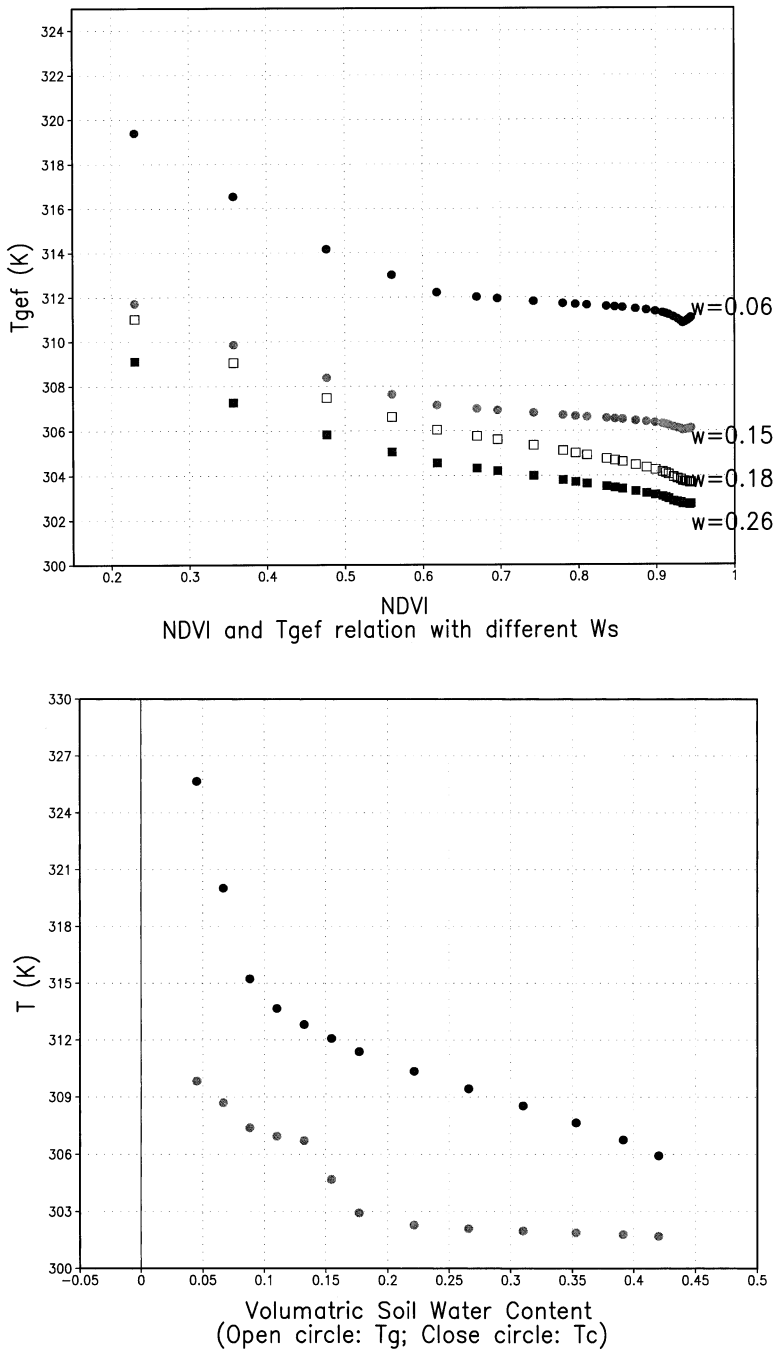

Fig. 4. (a) Variation of T_s as a function of vegetation cover as defined by the NDVI. Each line represents a different level of VSW (percent saturation). The $W=0.15$ represents the control experiment. Note the typical inverse relation between T_s and NDVI in comparison to the satellite observations in Fig. 2. (b) Variation of bare soil temperature (T_g) and canopy leaf temperature (T_c) as a function of varying VSW. Note the stepped increase of T_c at approximately 15% VSW. Stomatal closure occurs at this "wilting" point. (c) Variation of $\Delta T_{g,c}$ as a function of varying VSW. Note that as a result of the T_c stepped temperature, this TVX metric provides a poor diagnostic of soil moisture conditions.

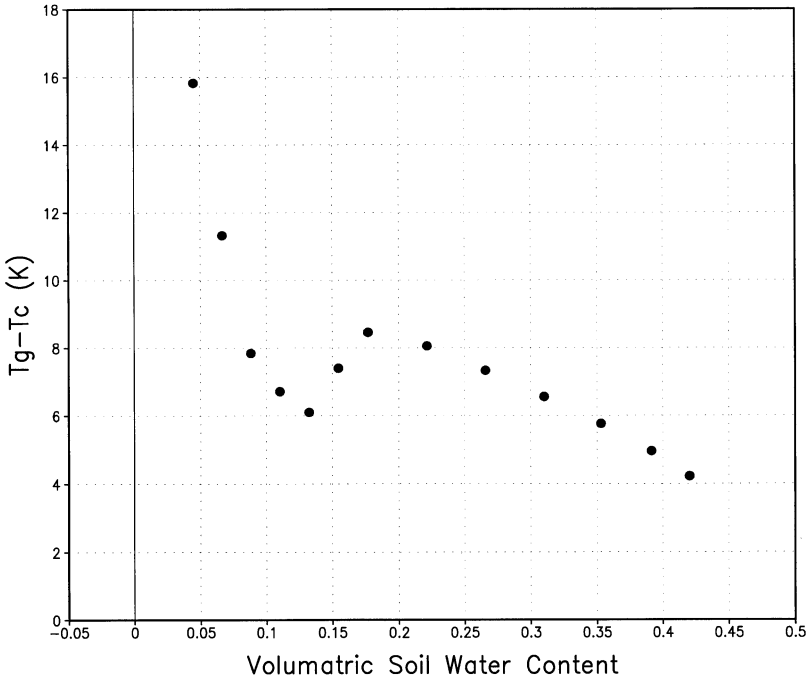

Fig. 4. *(continued)*

can be found in Goutorbe and Tarriea (1991). This site is a soybean crop field. Soybean plants start to grow in May and are harvested at the end of September.

This data set has been used for off-line model comparisons in the PILPS (Shao & Henderson-Sellers, 1996). Vegetation and soil parameters were provided by PILPS for this study. Fig. 8a shows the seasonal variation of LAI at HAPEX site. Observed precipitation, atmospheric temperature, wind speed, humidity, downward long-, and shortwave radiation from HAPEX-Mobilhy were used to drive land surface models (Fig. 8b–f). SSiB has participated in this comparison and produced reasonable results (Shao & Henderson-Sellers, 1996; Xue, Zeng, et al., 1996).

We selected to use this single observation site to carry out our modeling analyses because it is well characterized, providing the multiple model input parameters needed as well as measurements of the modeled prognostic variables. The soybean vegetation cover at this site is also quite simple and well understood. There has been considerable research on remote sensing of soybean crop canopies, which helps to simplify relating the model calculations and remotely sensed measurements.

3.3. Relation between LAI and remotely sensed NDVI

One of the difficulties in moving from field measurements and remotely sensed measurements is the relation between LAI and remotely sensed SVIs (Curran, 1980). For any given SVI, such as the NDVI, the relation is nonlinear and also varies with canopy leaf angle distribution. The most typical leaf angle distribution is "spherical" in which all angles of inclination are equally represented (Verhoeff, 1984). Soybean canopies are generally well represented by spherical canopy architectures (Badhwar, Verhoeff, & Bunnik, 1985).

For comparison to satellite observations, the model LAI measurements were converted to NDVI measurements with the following relation:

$$\mathrm{NDVI} = 0.095 - 0.89^{*}\exp(-\mathrm{LAI}) \quad (4)$$

This nonlinear relation was derived from calculations employing the SAIL vegetation canopy radiative transfer model for a spherical leaf angle distribution (Goward & Huemmrich, 1992). This LAI to NDVI conversion, expressive of Beers-type light attenuation in vegetation canopies, has the convenient attribute of producing a more nearly linear relation between T_s and the canopy foliar estimates, a characteristic noted in satellite TVX plots. Converting LAI to percentage canopy closure would produce a similar result.

4. Results

4.1. Sensitivity of TVX to environmental factors

In this section, we examine the sensitivity of the SSiB-calculated TVX patterns to environmental variations.

4.1.1. The testing methodology

To evaluate the underlying determinants of variations in the TVX metrics, model calculations were compiled for a typical day, with the diurnal forcing from midlatitude summer meteorological conditions for the HAPEX-Mobilhy site, including soil moisture, IR, temperature,

and wind at the reference height (Table 1). Precipitation was set to 0 to constrain the experiment. We refer to this analysis as our control experiment.

To derive the needed variations in vegetation canopy cover from 0% to 100% canopy closure, 30 individual model runs were completed. Each run evaluated one specific canopy cover condition defined by combination of values for LAI, vegetation cover, vegetation height, surface roughness length, and zero displacement height (Fig. 3). These canopy variations represent typical variations in canopy coverage that occur during different growth stages, as recorded in the field measurements.

This set of control calculations produced the expected TVX correlation between the vegetation canopy cover and surface temperature (Fig. 4a). In SSiB, surface temperature is evaluated from the upward long-wave flux, which is the effective radiative temperature (ERT) of the observed surface. If the surface is fully covered by the canopy, the ERT is the same as the canopy temperature. For bare ground, the ERT is in turn the same as the soil surface temperature. In between, it is a mix of the two surfaces based on relative contribution of long-wave radiation from each surface. Note that this is essentially identical with how the remote sensing instrument records T_s measurements from a combination of T_g and T_c land surface components. From these calculations, it is clear that the model replicates what is observed in remotely sensed TVX plots. Canopy NDVI and surface temperature are inversely related under identical daytime meteorological conditions. Increased LAI decreases surface temperature.

4.1.2. Influence of environmental factors on the TVX relation

We then conducted a sensitivity analysis in which soil moisture, IR, surface wind field, and atmospheric water vapor deficit were varied to test how the TVX patterns would change under these varying conditions (Table 1). To clearly understand the cause and effect of each parameter, only one variable was changed at a time in the sensitivity experiments. As noted in the control experiment, for each particular set of environmental conditions, we completed 30 separate model runs to capture the influence of varying vegetation cover. In total, over 1140 individual model runs were completed to produce the variance matrix of TVX metrics versus environmental conditions.

We display only the model results at 2 p.m. local time; an estimate of the conditions observed by the NOAA AVHRR PM sensors.

4.1.2.1. Soil moisture. The influence of variations in VSW on the TVX relation is dramatic (Fig. 4a and b). As soil water decreases, soil temperature (T_g) increases over 20 K, from 306 to 326 K. Canopy temperature (T_c) also increases from 302 to 310 K, however, T_c shows basically a stepped increase, at approximately 15% VSW, from 303 to 307 K. This stepped change occurs because the VSW has reached the "wilting point" where lack of soil water causes the plant stomata to close. These results indicate that variations of T_g may have some real value in estimating soil moisture status and that T_c may have some potential but only as an indicator of stomatal closure.

To confirm this perspective, we also forced stomata to remain open over the entire soil moisture range (Fig. 5a and b). Under this unrealistic scenario, T_c remains near 302 K throughout the entire VSW range. Essentially, all the TVX soil moisture information resides in the T_g variation in this case.

The stepped variation of T_c, with respect to soil moisture, as a result of stomatal closure, makes interpretation of $\Delta T_{c,g}$ (the difference between T_g and T_c and therefore the TVX slope) a poor diagnostic of surface moisture conditions. Note that $\Delta T_{c,g}$ takes on identical values for several widely differing values of VSW considered here (Fig. 4c). This result indicates that the slope of the TVX relation may not be a good indicator of soil moisture conditions, which contradicts previous analyses of the TVX relation (Carlson et al., 1994; Goward & Hope, 1989; Nemani & Running, 1989).

4.1.2.2. Incident radiation. Incident absorbed radiation is a primary determinant of surface temperatures, which in turn determines near-surface air and canopy temperatures (Geiger, 1965). We anticipated that the influence of net radiation would be at least as significant as soil moisture in producing variations in the TVX metrics. With satellite observations, complete assessment of net radiation (R_n) is more difficult to infer than the incident flux. As a result, in this study, we restricted our consideration to total incident (combined incoming long- and short-wave fluxes) rather than R_n, at the time of the observed T_s measurements.

We varied the incident radiant flux between 700 and 1400 W/m^2, which covers the range of incident radiance variations that would be experienced during the Spring, Summer, and Fall in this typical midlatitude location. The changes in the TVX metrics for variations in IR are nearly of the same magnitude as those observed for modeled soil moisture variations (Fig. 6a and b). The ground temperature increases from about 300 to over 318 K with increasing radiance under these conditions. The canopy temperature ranges from <300 to 308 K. The relations with T_g and T_c as well as $\Delta T_{c,g}$ are linear suggesting that addressing the radiation factor in TVX metrics may be straightforward (Gillies & Carlson, 1995).

Note that, at low IR, T_g and T_c are quite similar, <1 K different. This suggests that the precision of TVX metrics for estimating surface moisture conditions would be poor under low IR conditions, suggesting the limitations during the winter season or in summertime morning or evening hours.

4.1.2.3. Surface wind. Given the role of airflow on land/atmosphere energy balance, we anticipated that surface wind speed should play an important role in varying the TVX

relation as well. We considered a typical range of wind speeds expected during clear viewing conditions, in the range from 0.4 to 5 m/s. The results are somewhat surprising (Fig. 7a and b). The impact on increasing wind speed on T_g, over the range of wind speeds considered, is modest, decreasing T_g from 314 to 308 K or approximately 30% of the impact of either soil moisture or IR on variations in T_g. T_c decreases from 306 to 302 K or about 50% of the influence of the other two variables on T_c. Note that the influence of wind flow on the $\Delta T_{c,g}$ is quite small, about 2 K over the range of wind speeds considered.

These calculations suggest that airflow plays a modest but not insignificant role in determining the absolute values of T_g and T_c for given IR and soil moisture conditions. At the least, variations in wind speed will introduce some level of uncertainty in any derivation of soil moisture with the

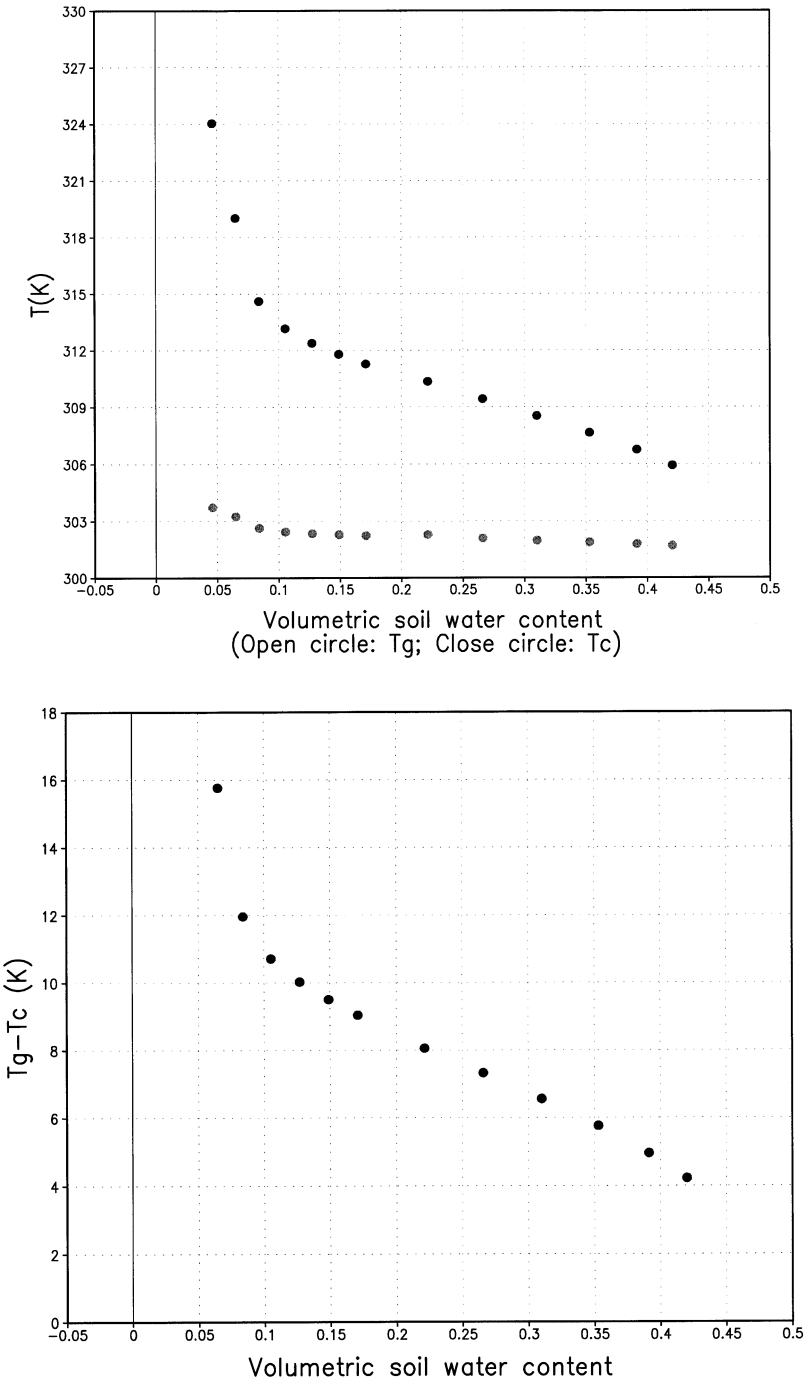

Fig. 5. (a) The same as Fig. 4b except the stomata remain open for all conditions of volumetric soil conditions. Under this unrealistic scenario, T_c remains nearly constant and T_g varies systematically with soil moisture. (b) The same as Fig. 4c but for the open stomata case. Here, $\Delta T_{g,c}$ does effectively track soil moisture, albeit in a nonlinear pattern. However, all of the variation in this TVX metric is then captured by variations on T_g.

TVX metrics. This outcome, of course, will also vary with IR conditions. Thus, during midgrowing season, variations in wind speed will be more important than at other times of the year.

4.1.2.4. Water vapor deficit. We also tested for the influence of surface water vapor deficit. Its impact is smaller (not shown) than wind speed and will not be investigated further in this paper.

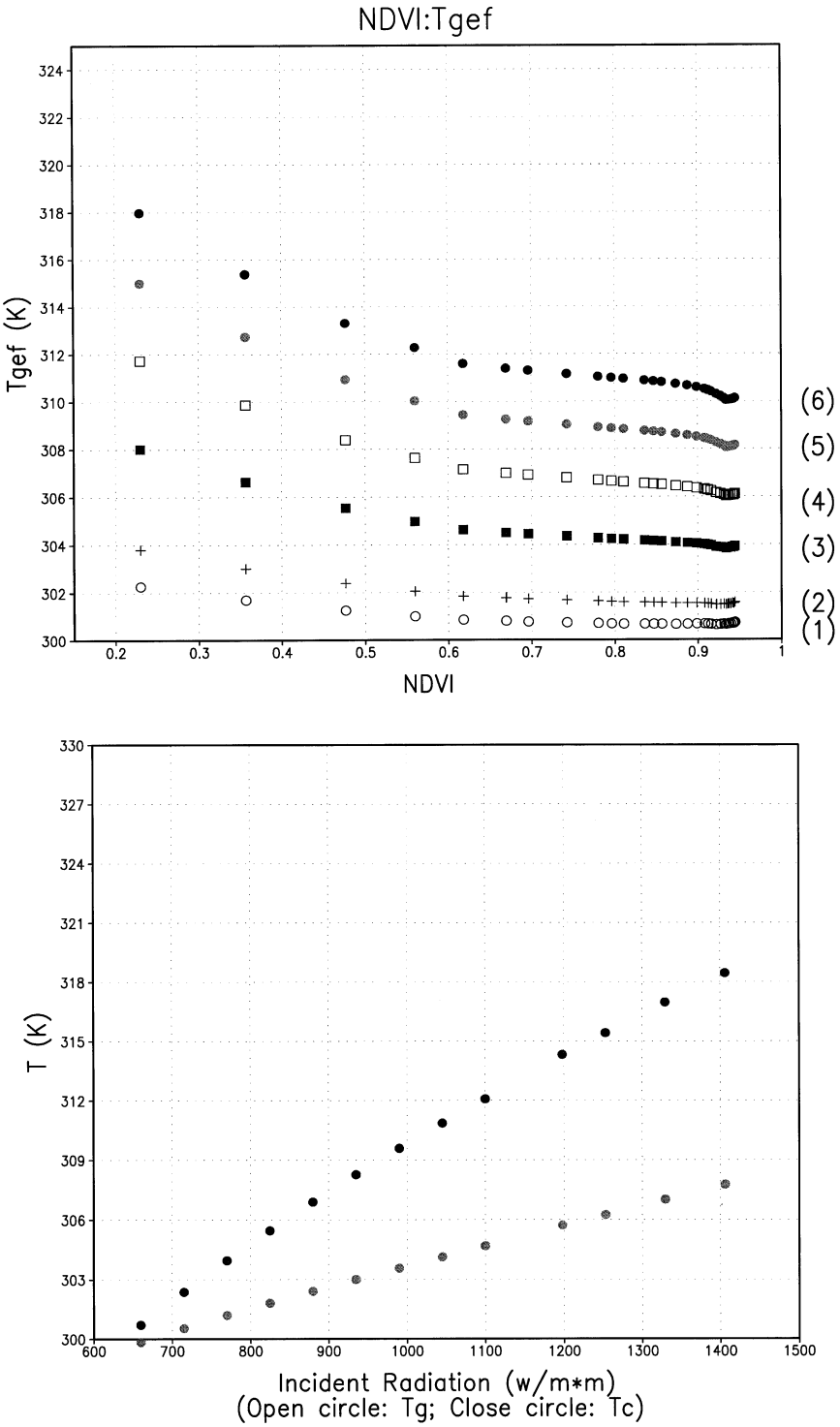

Fig. 6. (a) Variation of T_s as a function of NDVI. The six lines represent differing levels of incident downwelling radiation (short-wave plus long-wave), where (1) = 650 W/m^2 and (6) = 1400 W/m^2. (b) Variation of T_g and T_c as a function of incident downwelling radiation. Note the linear relation, suggestive of a possible simple adjustment factor.

4.2. Derivation of soil moisture from TVX metrics

In this section, we explore the use of TVX metrics to infer reported soil moisture variations at the Caumont site of the HAPEX-Mobilhy study area. Using the acquired ground measurements and SSiB, we compiled all of the relevant variables for the entire May to September growing season. We then statistically evaluated the relation between soil moisture, the TVX metrics, and other relevant variables. Based on the statistical results, we inferred soil moisture from the TVX metrics and compared the results with the reported weekly and modeled daily soil moisture conditions.

4.2.1. The experimental design

Our sensitivity analysis with SSiB indicated that the information derived from TVX metrics should provide a capability to evaluate surface moisture conditions, given knowledge of IR and wind speed. To evaluate this pos-

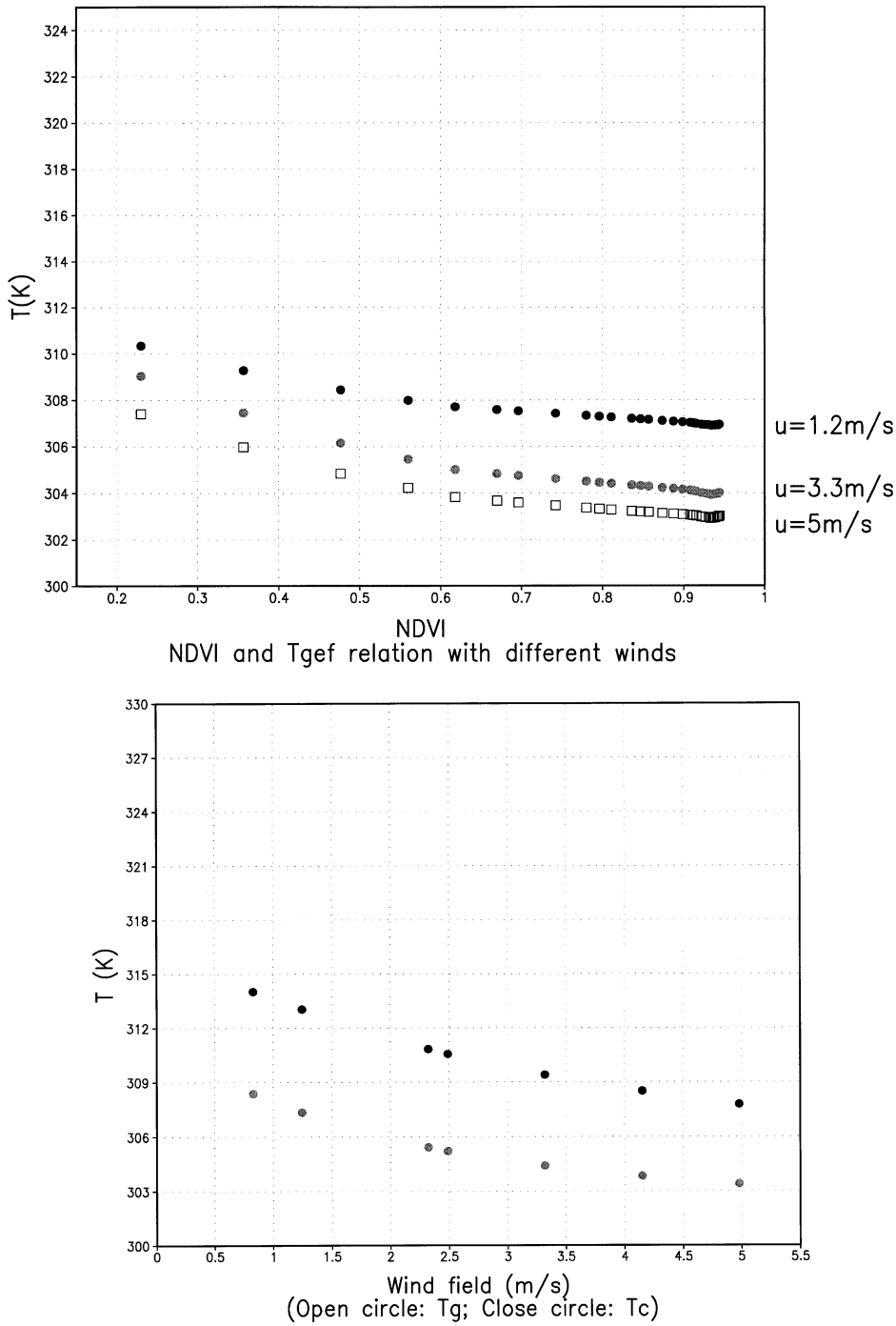

Fig. 7. (a) Variation of T_s as a function of NDVI for three wind speeds. (b) Variation of T_g and T_c as a function of wind speed.

Table 2
Environmental conditions observed at SAMER Site 3: May to September

	Minimum	Maximum
VSW	6%	27%
IR (w/m^2)	600	1200
Wind field (m/s)	1.0	4.00

sibility, we employed observational data from HAPEX-Mobilhy study to drive SSiB calculations through a typical growing season.

The measurements of soil moisture in HAPEX-Mobilhy were made using neutron sounding probes every week at every 0.1 m from the surface down to 1.6 m (Cuenca & Nolihan, 1991). These weekly measurements were compared with the SSiB calculations with good agreement (Xue, Zeng, et al., 1996). To increase our soil moisture observation frequency, we employed the SSiB computed daily soil moisture values. SSiB soil moisture was validated at the 10-cm depth, and then employed to also produce soil moisture conditions at 1 and 2 cm. As noted later, we found that the TVX metrics best represent the 2-cm soil moisture conditions, and therefore we focus on these results. However, a comparison with results at the 1- and 10-cm depths is also provided.

SSiB was integrated for 1 year with the meteorological data from the HAPEX-Mobilhly campaign. The time interval of the integration is 30 min. To avoid the spin up problem associated with soil moisture modeling, the model was first integrated for several years to reach equilibrium conditions. The soil moisture from the equilibrium calculations was used as the initial condition for the 1-year integration with the observed growing season conditions.

The precipitation, weekly soil moisture conditions, IR, and wind conditions were derived from the field observations. The daily soil moisture conditions, T_g and T_c at 2 p.m. local time, were derived from the off-line integration of the SSiB model. This collection of variables served as the basis for examining the quantitative relation between soil moisture, the TVX metrics, and the other relevant variables.

Because the precipitation has a great impact on the soil moisture and may contaminate the normal TVX/soil moisture relation, we restricted consideration to observations from days when there was no rain 6 h prior to 2 p.m. A total of 134 daily observations were available for analysis (from May through September) that passed this criterion.

Table 4
Multivariate analysis of soil moisture assessment

Case	Equation	R^2
1	$SM = 0.0827 - 0.0101*T_c + 0.0035T_g$	.65
2	$SM = 0.025 + 0.002*IR - 0.0114*T_g$	.70
3	$SM = 0.0532 - 0.0091*T_c + 0.0011*IR$	.72
4	$SM = 0.0381 - 0.0056*T_c - 0.0047T_g + 0.0016*IR$	.73
5	$SM = 0.0344 - 0.0048*T_c - 0.0071*T_g + 0.0020*IR - 0.0100u$	.75

The range of environmental conditions observed at the SAMER site approximate those conditions considered in the simulation analyses (Table 2).

The TVX metrics considered include T_c, T_g, and $\Delta T_{c,g}$, which estimates the slope of the T_s/NDVI relation. The end points of the TVX relation T_g and T_c were evaluated as noted in Eq. (4). Where LAI = 0, the NDVI will equal to 0.06, a value generally associated with nonvegetated surfaces. Full canopy closure typically occurs above a LAI of 3.0 for a spherical canopy. In this case, the NDVI is 0.9. As noted in Prihodko and Goward (1997), the T_g and T_c end point temperatures may be calculated by extrapolating the TVX measurements to the 0.06 and 0.9 NDVI values, so long as a reasonable range of NDVI measurements are included in the spatial/contextual array of remotely sensed observations.

4.2.2. The statistical relations

The basic correlation structure between TVX observables (T_g, T_c, and $\Delta T_{c,g}$) and environmental conditions (IR, wind speed, and soil moisture) for the SAMER site in most cases replicates the relations noted in the sensitivity analysis (Table 3).

T_g and T_c are strongly positively correlated (.89). They are negatively related to soil moisture and positively related to IR. Note that there is a weak positive relation between soil moisture and IR (.11), reflecting the seasonal trends in these two variables. The relations of T_g and T_c with wind speed are negative and modest. Variations in wind speed explain $<19\%$ of the variance observed in either variable. Note that the relation between $\Delta T_{c,g}$ and soil moisture is also weak, explaining only 6% of the variance in soil moisture, again, confirming the sensitivity analysis.

The basic correlation structure of the variables indicates that either T_g or T_c may provide a suitable diagnostic for near-surface soil moisture conditions but not the TVX slope.

Table 3
Explained variance (R^2) between variables at the SAMER site

	IR	Wind speed	Soil moisture	T_g	T_c	$\Delta T_{c,g}$
IR	–	.02	.11 (−.34)	.68 (.82)	.46 (.68)	.19 (.44)
Wind speed	.02	–	.11 (−.34)	.19 (−.44)	.18 (−.43)	.0
Soil moisture	.11 (−.34)	.11 (−.34)	–	.5 (−.70)	.63 (−.80)	.06 (.25)
T_g	.68 (.82)	.19 (−.44)	.5 (−.70)	–	.89 (.94)	.03
T_c	.46 (.68)	.18 (−.43)	.63 (−.80)	.89 (.94)	–	.02
$\Delta T_{c,g}$	.19 (.44)	.0	.06 (.25)	.03	.02	–

The numbers in parentheses are correlation.

Table 5
Predictive capacity of T_c, T_g, and IR regression equations for soil moisture assessment

Soil depth	Explained variance (correlation)	Explained variance by climate mean	Residual standard error
10 cm	.69 (.83)	.28	.05
2 cm	.77 (.88)	.29	.04
1 cm	.77 (.88)	.30	.04
2 cm (with U)	.79 (.89)	.29	.03

However, the additional correlation of T_g and T_c to IR and, to a lesser degree, wind speed, suggest the need for a multivariable solution for estimating soil moisture. To evaluate this possibility, we considered a series of multiple stepwise regressions to assess the relative importance of accounting for each of the multiple factors (Table 4).

Interestingly, the combination of T_c and T_g in a multivariate equation improves the explained variance by 15% (.65) over T_g alone and 3% over T_c alone. Note that the regression equation evaluates the contrast between T_g and T_c, suggesting that some scaled assessment of $\Delta T_{c,g}$ may in fact improve analysis of soil moisture conditions. However, contrary to the sensitivity model analyses, in this case, the variations in T_c are the dominant explanatory factor, subject to small adjustments for T_g. This suggests that T_g is adjusting for other environmental conditions. The strong positive correlation of T_g with IR may explain why T_g serves to adjust the T_c values in this equation.

The inclusion of IR with either T_g or T_c improves the soil moisture explained variance to over 70%, with the T_c, IR equation 2% better than the T_g, IR equation. This indicates that adjusting either T_g or T_c for IR conditions substantially improves (8% over T_c alone and 20% over T_g alone) the value of these TVX metrics in evaluating soil moisture conditions. Inclusion of both T_g and T_c with IR further increases the explained variation another 1–3% to 73% and including wind speed increases the explained variation to 75%.

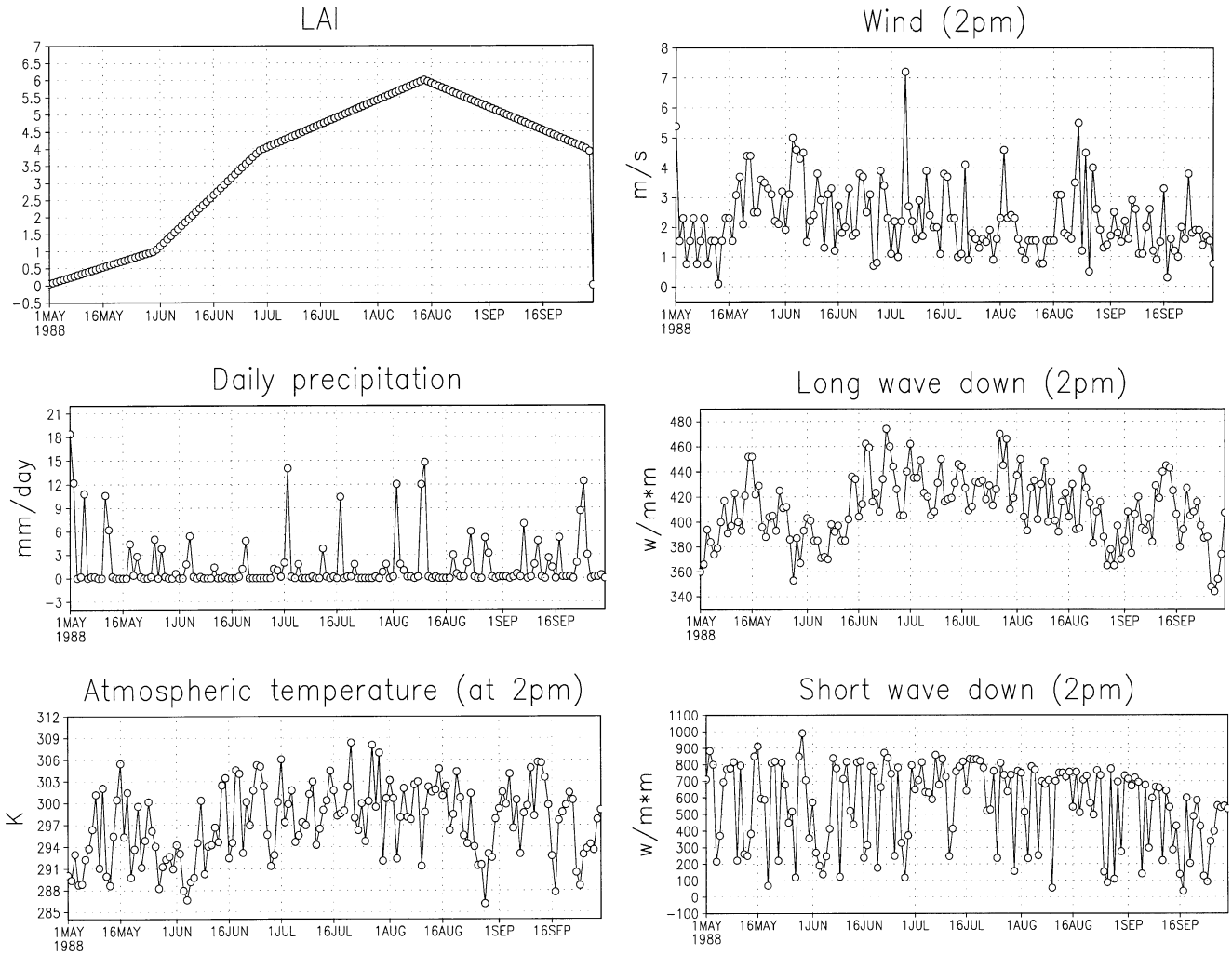

Fig. 8. The forcing variables employed to examine TVX metrics for the HAPEX-Mobilhy study site. (a) LAI, (b) precipitation, (c) 2 p.m. atmospheric temperature, (d) 2 p.m. wind flow, (e) long-wave IR, (f) short-wave IR.

Clearly, the majority of the soil moisture information potential originates from the T_g and T_c TVX metrics and knowledge of IR does improve the use of the metrics in assessing soil moisture conditions. The modest 2% increment from knowledge of wind speed adds little to the explanatory value of this approach.

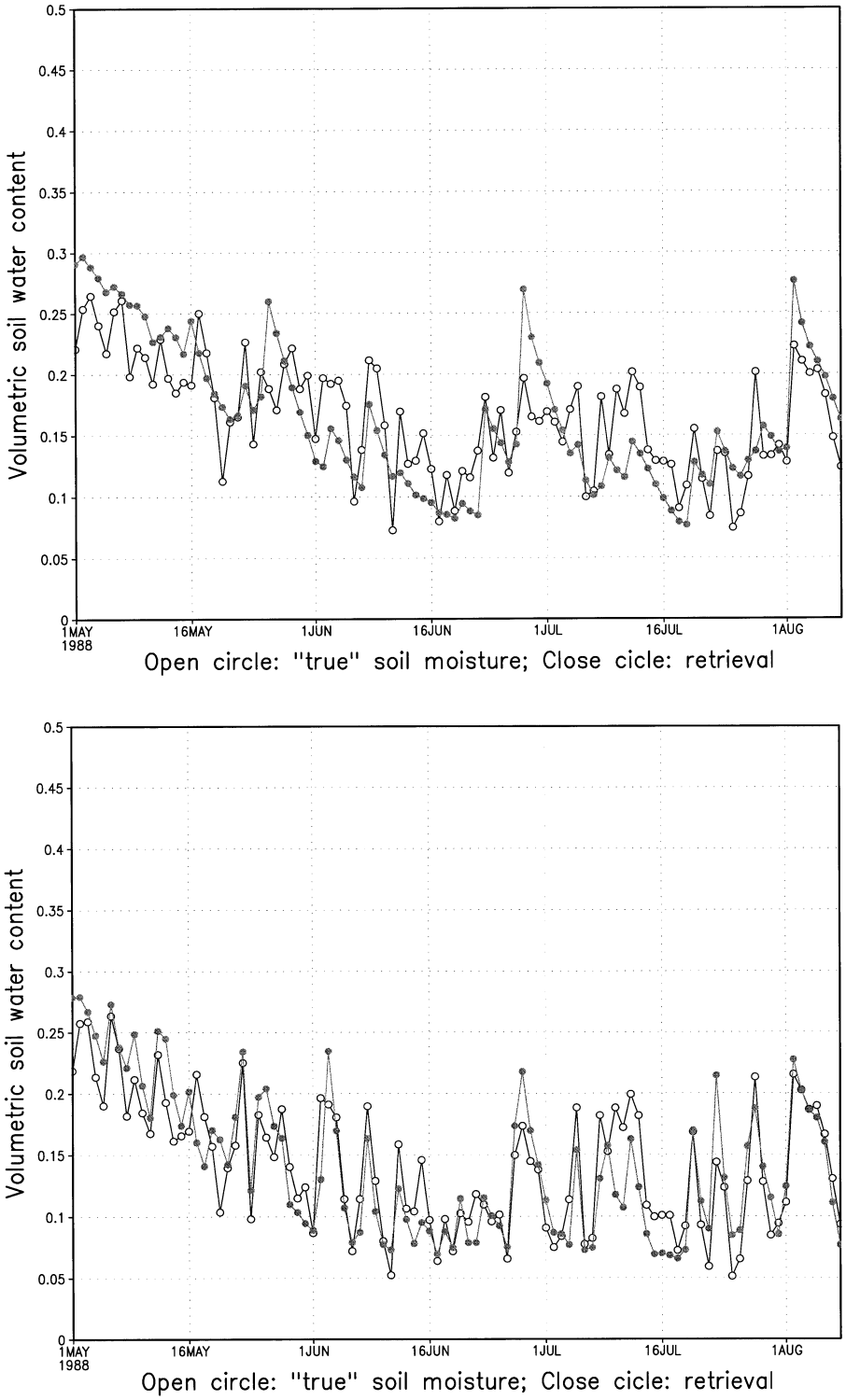

Fig. 9. (a) Soil moisture retrieval for 10-cm soil moisture using the Case 4 multivariate regression equation, which includes T_g, T_c, and incident downwelling radiation. The open circles are the retrieval versus the modeled *actual* 10-cm conditions. Note that the retrievals tend to overshoot the actual conditions. (b) Same as (a) but for the 2-cm depth modeled soil moisture. Note that in this case the retrievals are much closer to the modeled *actual* conditions. A similar analysis for 1 cm showed little further improvement.

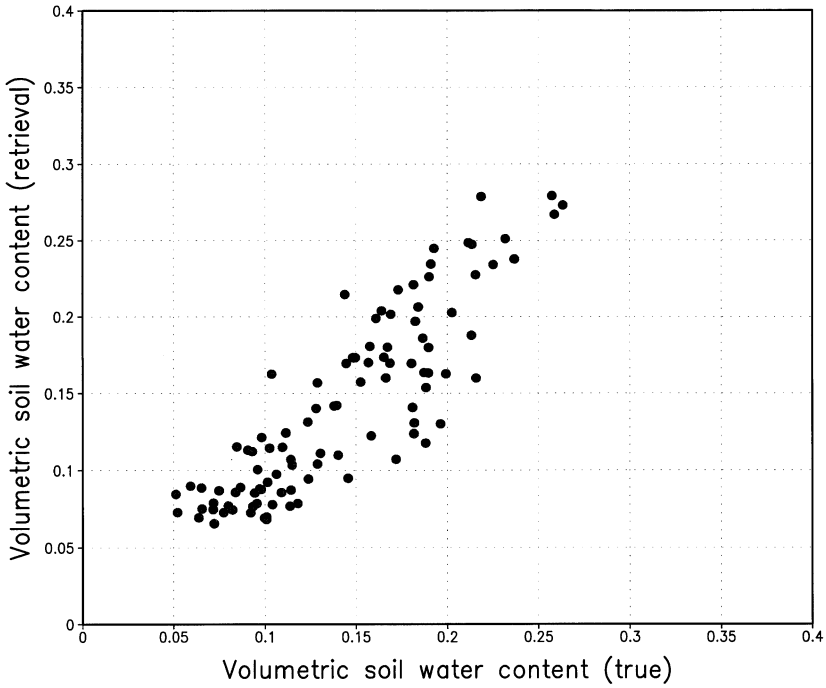

Fig. 10. Scatterplot of the retrieved versus actual soil moisture conditions for the entire observation period. A general linear relation is noted with a residual standard error of <4% VSW over a range of 6–27% VSW.

4.2.3. Soil moisture assessment with statistical equations

Based on our statistical results and our known capacity to estimate the relevant environmental variables with satellite observations, we employed the Case 4 regression equation, including T_g, T_c, and IR to predict 2-cm depth soil moisture conditions at the HAPEX-Mobilhy site (Table 5). We also

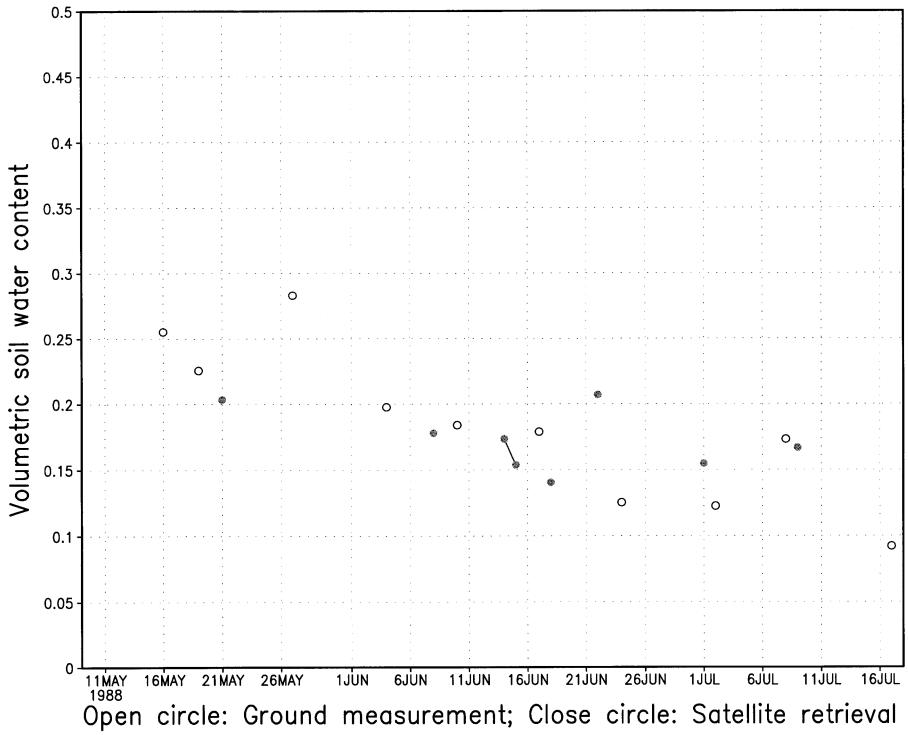

Fig. 11. AVHRR sensor retrieval of soil moisture for seven overpasses during the HAPEX-Mobilhy study. Filled circles represent the satellite retrievals. The open circles are reported near-surface soil moisture measurements. The general trends look encouraging but more intensive exploration of the method will be needed to fully demonstrate the approach.

pursued statistical analyses to evaluate soil moisture conditions at 1- and 10-cm depths. In these experiments, we set the depth of first soil layer as 1 and 10 cm, respectively, and repeated the procedures discussed above to generate regression equations similar to the one for Case 4. We then used these equations to predict the soil moisture at 1 and 10 cm. This aspect of the analysis was undertaken to assess how well the TVX metric represent soil moisture conditions at these different depths.

For all cases, the regression equations produced reasonable predictions of the seasonal and short-term variations in soil moisture (Table 5) (Fig. 9a and b). The predicted soil moisture shows the same spring dry down and short-term recharge events as the true soil moisture. At 10-cm soil depth, TVX captures much of the seasonal trend but is less successful with short-term variations (Fig. 9a). The results for 2-cm depth more closely track the short-term variations. Little improvement was observed for the 1-cm depth analysis (not shown). Note that the prediction errors are larger during May, when the soil moisture is drying out. If the May prediction is excluded, the RMS error is 0.03 VSW (Fig. 10).

4.3. Satellite retrievals

We tested the satellite soil moisture retrieval algorithm with AVHRR data from the HAPEX-Mobilhy site (Andre', Goutorbe, & Perrier, 1986). The images used in this study correspond to a special observation period (SOP) 1 May 1986 to 15 July 1986 for which six completely clear images were available.

The eight-bit digital numbers for each channel were calibrated and converted to reflectance in Channels 1 and 2 (visible and near infrared) and temperature in Channels 4 and 5 (thermal infrared) using equations developed for NOAA-9 data. Channels 1 and 2 were used to calculate the NDVI that was then used to calculate LAI (Eq. (4)) for each pixel within the satellite image. Land surface temperature was calculated using a second order split window equation using brightness temperatures from AVHRR Channels 4 and 5 with coefficients derived by Ouaidrari, Czajkowski, Goward, Sobrino, and Vermote (2000). The TVX algorithm was applied to the center of a 9×9 pixel moving window to find T_g and T_c.

For the selected scenes, we employed satellite-derived T_g and T_c using the TVX methodology, along with ground measurements of IR to estimate 2-cm soil moisture conditions during the dates of the satellite over passes. T_g and T_c were found by extending the TVX slope for each 9×9 window to an NDVI of 0.06 for T_g and 0.9 for T_c. The soil moisture values corresponding to the locations of the ground observation stations were extracted and compared to values derived from the equation for Case 4 (Table 4). The results, although sparse in fact do capture the seasonal trend, and in all but one case, closely approximate the conditions recorded on the ground for that date (Fig. 11).

These results are encouraging but offer far too few comparative points to convincingly demonstrate potential for these satellite observations to monitor surface soil moisture conditions. We are currently exploring the use of the Oklahoma Mesonet as a means to more fully test this approach.

5. Conclusions

The results from this analysis suggest that the slope of the TVX relation may be of less value to assessment of soil moisture conditions than the end points of this relation, as measures of closed canopy (T_c) and bare ground (T_g) conditions. Adjustment of these metrics for IR conditions at the time of the observations enhances the quality of the soil moisture assessments derived from the remotely sensed variables. Including IR measurements improved our assessments by nearly 10%.

In this study, we pursued a model-based statistical analysis to evaluate the potential of TVX metrics in this important application. The results are therefore specific to this model and the study site observations employed. A more generalized physical model of how to employ remotely sensed TVX metrics will be required to employ this approach at regional and global scales.

The largest remaining uncertainty in this analysis is the degree to which the model replicates the full complexity of vegetation canopy conditions observed by satellite remote sensing systems. Our limited analysis of actual AVHRR observations produced encouraging results but the temporal density of the observations is not sufficient to develop full confidence in this statistically derived model-based approach. One of the more intriguing aspects of our results is the observed T_c step-function that results from stomatal closure. With a "big-leaf" model such as SSiB, this phenomenon may well dominate the calculations, whereas in a real vegetation canopy other factors such as leaf wilt or reorientation may be more significant.

As interesting and encouraging as these results are, they leave many critical questions unanswered. With the advent of the new generation of EOS sensors, including Landsat-7, ASTER, and MODIS, it may now be possible to explore these questions more fully. This study lays some of the groundwork for such investigations in the future.

Acknowledgments

This study was carried with support of grants from the National Aeronautics and Space Administration, Earth Science Enterprise Office, grant NAG5-7587 and the National Oceanic and Atmospheric Administration, grant NA76GP0397. We would also like to thank Drs. Shunlin Liang and Hassan Ouaidrari for their assistance in carrying out various aspects of the analysis presented.

References

Anderson, M. C., Norman, J. M., Diak, G. R., Kustas, W. P., & Mecikalski, J. R. (1997). A two-source time-integrated model for estimating surface fluxes using thermal infrared remote sensing. *Remote Sensing of Environment*, *60*, 195–216.

Andre', J.-C., Goutorbe, J.-P., & Perrier, A. (1986). HAPEX-Mobilhy: a hydrologic atmospheric experiment for the study of water budget and evaporation flux at the climatic scale. *Bulletin of the American Meteorological Society*, *67*, 138–144.

Badhwar, G. D., Verhoeff, W., & Bunnik, J. J. (1985). Comparative study of suits and SAIL canopy reflectance models. *Remote Sensing of Environment*, *17*, 179–195.

Carlson, T. N., Dodd, J. K., Benjamin, S. G., & Cooper, J. N. (1981). Satellite estimation of surface energy balance, moisture availability and thermal inertia. *Journal of Applied Meteorology*, *20*, 67–87.

Carlson, T. N., Gilles, R. R., & Perry, E. M. (1994). A method to make use of thermal infrared temperature and NDVI measurements to infer surface soil water content and fractional vegetation cover. *Remote Sensing Reviews*, *9*, 161–173.

Carlson, T. N., Perry, E. M., & Schmugge, T. J. (1990). Remote estimation of soil moisture availability and fractional vegetation cover for agricultural fields. *Agricultural and Forest Meteorology*, *52*, 45–69.

Chanzy, A., Bruckler, L., & Perrier, A. (1995). Soil evaporation monitoring: a possible synergism of microwave and infrared remote sensing. *Journal of Hydrology*, *165*, 235–259.

Chen, D., Engman, E. T., & Brutsaert, W. (1997). Spatial distribution and pattern persistence of surface soil moisture and temperature over prairie from remote sensing. *Remote Sensing of Environment*, *61*, 347–360.

Chen, F., Mitchell, K., Schaake, J., Xue, Y., Pan, H.-L., Koren, V., Duan, Q., Ek, M., & Betts, A. (1996). Modeling of land-surface evaporation by four schemes and comparison with FIFE observations (PILPS). *Journal of Geophysical Research*, *101* (D3), 7251–7268.

Chen, T. H., et al. (1997). Cabauw experimental results from the project for inter-comparison of land surface parameterization schemes. *Journal of Climate*, *10*, 1194–1215.

Cooper, D. I., & Asrar, G. (1989). Evaluating atmospheric correction models for retrieving surface temperatures from the AVHRR over a tall grass prairie. *Remote Sensing of Environment*, *27*, 93–102.

Cuenca, R. H., & Nolihan, J. (1991). Use of soil moisture measurement. In: J. Schmugge, & J. Andre (Eds.), *Land surface evaporation* (pp. 287–299). Berlin: Springer.

Curran, P. J. (1980). Multispectral remote sensing of vegetation amount. *Progress in Physical Geography*, *4*, 175–184.

Curran, P. J. (1981). The estimation of surface moisture of a vegetated soil using aerial infrared photography. *International Journal of Remote Sensing*, *2*, 369–378.

Curran, P. J. (1983). Multispectral remote sensing for estimation of green leaf area index. *Philosophical Transactions of the Royal Society, Series A*, *309*, 257–270.

Czajkowski, K., Goward, S. N., Chilar, J., Dubayah, R., & Mulhern, T. (1997). Biospheric Environmental Monitoring at BOREAS with AVHRR observations. *Journal of Geophysical Research*, *102* (D24), 29651–29662.

Czajkowski, K., Goward, S. N., Stadler, S., & Waltz, A. (2000). Thermal remote sensing of near surface environmental variables: application over the Oklahoma Mesonet. *The Professional Geographer*, *52*, 345–357.

Dubayah, R., Wood, E. F., & Lavallee, D. (1996). Multiscaling analysis in distributed modeling and remote sensing: an application using soil moisture. In: D. Quartrochhi, & M. Goodchild (Eds.), *Scale in remote sensing and GIS* (pp. 93–112). New York, NY: Lewis.

Engman, E. T., & Chauhan, N. (1997). Status of microwave soil moisture measurements with remote sensing. *Remote Sensing of Environment*, *51*, 189–198.

Friedl, M. A., & Davis, F. W. (1994). Sources of variation in radiometric surface temperature over a tallgrass prairie. *Remote Sensing of Environment*, *48*, 1–17.

Geiger, R. (1965). *Climate near the ground*. Cambridge, MA: Harvard University Press.

Gillies, R. R., & Carlson, T. N. (1995). Thermal remote sensing of surface soil water content with partial vegetation cover for incorporation into climate models. *Journal of Applied Meteorology*, *34*, 745–756.

Goetz, S. J. (1997). Multi-sensor analysis of NDVI, surface temperature and biophysical variables at a mixed grassland site. *International Journal of Remote Sensing*, *18* (1), 71–94.

Goutorbe, J. P., & Tarriea, C. (1991). HAPEX-Mobilhy data base. In: Schmugge, & Andre (Eds.), *Land surface evaporation* (pp. 171–182). Berlin: Springer.

Goward, S. N., Cruickshanks, G. C., & Hope, A. S. (1985). Observed relation between thermal emissions and reflected spectral reflectance from a complex vegetated landscape. *Remote Sensing of Environment*, *18*, 137–146.

Goward, S. N., & Hope, A. S. (1989). Evapotranspiration from combined reflected solar and emitted terrestrial radiation: preliminary FIFE results from AVHRR data. *Advances in Space Research*, *9* (7), 239–249.

Goward, S. N., & Huemmrich, K. F. (1992). Vegetation canopy PAR absorptance and the normalized difference vegetation index: an assessment using the SAIL model. *Remote Sensing of Environment*, *39*, 119–140.

Goward, S. N., Waring, R. H., Dye, D. G., & Yang, J. (1994). Ecological remote sensing at OTTER: macroscale satellite observations. *Ecological Applications*, *4* (2), 322–343.

Hardy, J. R. (1980). Survey of methods for the determination of soil moisture content by remote sensing methods. In: G. Fraysse (Ed.), *Remote sensing applications in agriculture and hydrology* (pp. 233–247). Rotterdam: A.A. Balkema.

Hatfield, J. L. (1979). Canopy temperatures: the usefulness and reliability of remote measurements. *Agronomy Journal*, *71*, 889–892.

Heilman, J. L., Kanemasu, E. T., Rosenberg, N. J., & Blad, B. L. (1976). Thermal scanner measurement of canopy temperatures to estimate evapotranspiration. *Remote Sensing of Environment*, *5*, 127–145.

Henderson-Seller, A., & Brown, V. B. (1992). Project for Intercomparison of Land-Surface Parameterization Scheme (PILPS). *IGPO Publication Series*, *5*, 32.

Holben, B. N., Tucker, C. J., & Fan, C. J. (1980). Assessing soybean leaf area and leaf biomass with spectral data. *Photogrammetric Engineering*, *46*, 651–656.

Hope, A. S., & McDowell, T. P. (1992). The relationship between surface temperature and a spectral vegetation index of a tallgrass prairie: effects of burning and other landscape controls. *International Journal of Remote Sensing*, *13* (15), 2849–2863.

Hope, A. S., Petzold, D. E., Goward, S. N., & Ragan, R. M. (1987). Simulating canopy reflectance and thermal infrared emissions for estimating evapotranspiration. *Water Resources Bulletin*, *22* (6), 1011–1019.

Hunt, G. E. (1973). Radiative properties of terrestrial clouds at visible and infrared thermal wavelengths. *Quarterly Journal of Royal Meteorological Society*, *99*, 345–369.

Jackson, R. D. (1983). Spectral indices in n-space. *Remote Sensing of Environment*, *13*, 1401–1429.

Kasischke, E. S., Melack, J. M., & C., D. M. (1997). The use of imaging radars for ecological applications—a review. *Remote Sensing of Environment*, *59*, 141–156.

Kustas, W. P., Perry, E. M., Doriswamy, P. C., & Moran, M. S. (1994). Using satellite remote sensing to extrapolate evapotranspiration estimates in time and space over a semiarid rangeland basin. *Remote Sensing of Environment*, *49*, 275–286.

Moran, M. S., Vidal, A., Troufleau, D., Qi, J., Clarke, T. R., Pinter, P. J. Jr., Mitchell, T. A., Inoue, Y., & Neale, M. U. (1997). Combining multifrequency macrowave and optical data for crop management. *Remote Sensing of Environment*, *61*, 96–109.

Nemani, R., Pierce, L., Running, S., & Goward, S. N. (1993). Developing

satellite-derived estimates of surface moisture status. *Journal of Applied Meteorology*, *32* (3), 548–557.

Nemani, R. R., & Running, S. W. (1989). Estimation of surface resistance to evapotranspiration from NDVI and thermal-IR AVHRR data. *Journal of Climate and Applied Meteorology*, *28*, 276–294.

Njoku, E. G., & Entekhabi, D. (1996). Passive microwave remote sensing of soil moisture. *Journal of Hydrology*, *184*, 101–129.

Norman, J. M., Divakarla, J., & Goel, N. S. (1995). Algorithms for extracting information from remote thermal-IR observations of the Earth's surface. *Remote Sensing of Environment*, *51*, 157–169.

Ouaidrari, H., Czajkowski, K. P., Goward, S. N., Sobrino, J. A., & Vermote, E. (2000). Land surface temperature estimation from AVHRR thermal infrared measurements: an assessment for the AVHRR land Pathfinder II data set. *Journal of Geophysical Research* (in review).

Price, J. C. (1980). The potential of remotely sensed data to infer surface soil moisture and evaporation. *Water Resources Research*, *16*, 787–795.

Price, J. C. (1990). Using spatial context in satellite data to infer regional scale evapotranspiration. *IEEE Transactions on Geosciences and Remote Sensing*, *28* (5), 940–948.

Prihodko, L., & Goward, S. N. (1997). Estimation of air temperature from remotely sensed observations. *Remote Sensing of Environment*, *60* (3), 335–346.

Robock, A., Vinnikov, K. V., Schlosser, C. A., Speranskaya, N. A., & Xue, Y. (1995). Use of Russian soil moisture and meteorological observations to validate soil moisture simulations with biosphere and bucket models. *Journal of Climate*, *8*, 15–35.

Schlosser, C. A., Robock, A., Vinnikov, K. Y., Speranskaya, N. A., & Xue, Y. (1997). 18-year land-surface hydrology model simulations for a midlatitude grassland catchment in Valdai, Russia. *Monthly Weather Review*, *125*, 3279–3296.

Sellers, P. J., & Schimel, D. S. (1993). Remote sensing of the land biosphere and biogeochemistry in the EOS era: science priorities, methods and implementation. *Global and Planetary Change*, *7*, 279–297.

Shao, Y., & Henderson-Sellers, A. (1996). Validation of soil moisture simulation in land surface parameterization schemes with HAPEX data. *Global Planet Change*, *13*, 11–46.

Smith, J. A., Ranson, K. J., Nguyen, D., & Balick, L. (1985). Thermal vegetation canopy model studies. *Remote Sensing of Environment*, *11*, 26–31.

Smith, R. C. G., & Choudhury, B. J. (1991). Analysis of normalized difference and surface temperature observations over southeastern Australia. *International Journal of Remote Sensing*, *12* (10), 2021–2044.

Theis, S. W., Blancher, B. J., & Newton, R. W. (1984). Utilization of vegetation indices to improve microwave soil moisture estimates over agricultural lands. *IEEE Transactions on Geosciences and Remote Sensing*, *GE-22*, 490–496.

Tucker, C. J. (1979). Red and photographic infrared linear combinations for monitoring vegetation. *Remote Sensing of Environment*, *8*, 127–150.

Verhoeff, W. (1984). Light scattering by leaf layers with application to canopy reflectance modeling: the SAIL model. *Remote Sensing of Environment*, *16*, 125–141.

Wood, E. F. (1997). Effects of soil moisture aggregation on surface evaporative fluxes. *Journal of Hydrology*, *190*, 397–412.

Wood, E. F., et al (1998). The Project for Intercomparison of Land-Surface Parameterizations Schemes (PILPS) Phase-2(c) Red-Arkansas River Basin experiment: 1. Experiment description and summary intercomparisons. *Global and Planetary Change*, *19*, 115–135.

Xue, Y., Allen, S. J., & Li, Q. (1996). Sahel drought and land surface processes—a study using SEBEX and HAPEX-Sahel Data. Preprint of Second International Scientific Conference on the Global Energy and Water Cycle, 11–12.

Xue, Y., Bastable, H. G., Dirmeyer, P. A., & Sellers, P. J. (1996). Sensitivity of simulated surface fluxes to changes in land surface parameterization—a study using ABRACOS data. *Journal of Applied Meteorology*, *35,* 386–400.

Xue, Y., Sellers, P. J., Kinter, J. L. III, & Shukla, J. (1991). A simplified biosphere model for global climate studies. *Journal of Climate*, *4*, 345–364.

Xue, Y., Zeng, F. J., & Schlosser, C. A. (1996). SSiB and its sensitivity to soil properties — a case study using HAPEX-Mobilhy data. *Global and Planetary Change*, *13*, 183–194.

Xue, Y., Zeng, F. J., Schlosser, C. A., & Allen, S. (1998). A simplified Simple Biosphere Model (SSiB) and its application to land–atmosphere interactions. *Chinese Journal of Atmospheric Sciences*, *22*, 468–480.